Night-time chemistry of biomass burning emissions in urban areas: A dual mobile chamber study

Spiro D. Jorga[1], Kalliopi Florou[2], Christos Kaltsonoudis[2], John K. Kodros[2], Christina Vasilakopoulou[2,3], Manuela Cirtog[5], Axel Fouqueau[6], Bénédicte Picquet-Varrault[5], Athanasios Nenes[2,4], and Spyros N. Pandis[1,2,3]

[1]Department of Chemical Engineering, Carnegie Mellon University, Pittsburgh, 15213, USA

[2]Institute of Chemical Engineering Sciences, ICE-HT, Patras, 26504, Greece

[3]Department of Chemical Engineering, University of Patras, Patras, 26504, Greece

[4]School of Architecture, Civil & Environmental Engineering, Ecole Polytechnique Federale de Lausanne, Lausanne, 1015, Switzerland

[5]LISA, UMR CNRS 7583, Université Paris-Est Créteil, Université de Paris, Institut Pierre Simon Laplace (IPSL), Créteil, France

[6]Laboratoire National de Métrologie et d'Essais (LNE), 75015 Paris, France

Correspondence to: Spyros N. Pandis (spyros@chemeng.upatras.gr)

Abstract

Residential biomass burning for heating purposes is an important source of air pollutants during winter. Here we test the hypothesis that significant secondary organic aerosol production can take place even during winter nights through oxidation of the emitted organic vapors by the nitrate (NO_3) radical produced during the reaction of ozone and nitrogen oxides. We use a mobile dual smog chamber system which allows the study of chemical aging of ambient air against a control reference. Ambient urban air sampled during a wintertime campaign during night-time periods with high concentrations of biomass burning emissions was used as the starting point of the aging experiments. Biomass burning organic aerosol (OA) was on average 70% of the total OA in the beginning of our experiments. Ozone was added in the perturbed chamber to simulate mixing with background air (and subsequent NO_3 radical production and aging), while the second chamber was used as a reference. Following the injection of ozone, rapid OA formation was observed in all experiments leading to increases of the OA concentration by 20-70%. The oxygen-to-carbon ratio of the OA increased on average by 50% and the mass spectra of the produced OA was quite similar to the oxidized OA mass spectra reported during winter in urban areas. Further, good correlation was found for the OA mass spectra between the ambient-derived emissions in this study and the nocturnal aged laboratory-derived biomass burning emissions from previous work. Concentrations

33   of NO$_3$ radicals as high as 25 ppt were measured in the perturbed chamber with an accompanying
34   production of 0.1-3.2 µg m^{-3} of organic nitrate in the aerosol phase. Organic nitrate represented
35   approximately 10% of the mass of the secondary OA formed. These results strongly indicate that
36   the OA in biomass burning plumes can chemically evolve rapidly even during wintertime periods
37   with low photochemical activity.

38

39   **1. Introduction**

40   Biomass burning from residential heating, agricultural fires, prescribed burning, and
41   wildfires is a major source of atmospheric pollutants worldwide (Watson 2002, Bond et al. 2004,
42   Robinson et al. 2006). Emissions from biomass burning contribute both primary organic aerosol
43   (POA) and organic vapors that upon further reactions in the atmosphere can produce secondary
44   organic aerosol (SOA) (Andreae & Merlet 2001, Akagi et al., 2011, Bruns et al., 2016, Akherati
45   et al., 2020). The use of wood burning for domestic heating purposes is one of the major sources
46   of OA in many countries and is a major contributor to the violation of daily PM standards in
47   European cities (Alfarra et al., 2007, Favez et al., 2010, Fuller et al., 2014). Biomass burning
48   emissions and their products have significant but still uncertain impacts on human health and
49   climate (Ford et al., 2018; O'Dell et al., 2019).

50   The organic aerosol emitted during biomass burning undergoes extensive physical and
51   chemical changes in the atmosphere. More volatile components evaporate as emissions dilute in
52   the atmosphere (Tkacik et al., 2017); these semivolatile organic compounds (SVOCs) together
53   with the other emitted intermediate volatility (IVOCs) and volatile organic compounds (VOCs)
54   are subsequently oxidized leading to the production of SOA. Photochemical oxidation of biomass
55   burning emissions and the resulting SOA production have been studied both in the laboratory
56   (Hennigan et al., 2011; Ortega et al., 2013; Tkacik et al., 2017; Ahern et al.; 2019; Kodros et al.,
57   2020) and in the field (Capes et al., 2008; Jolleys et al., 2015; Vakkari et al., 2018). The reactions
58   of VOCs, IVOCs and SVOCs with the OH radical are considered to be the dominant chemical
59   pathway for oxidation, but reactions of emitted monoterpenes with ozone can also contribute to
60   the SOA formation during the chemical aging of biomass burning emissions (Yu et al., 1999, Zhao
61   et al., 2015). Despite considerable uncertainties remaining on the amount of SOA that can be
62   produced, and the net change of the biomass burning OA concentration when evaporation is

63 considered, it is clear that this daytime processing is important for converting the fresh biomass
64 burning OA to oxidized OA (OOA) (Bougiatioti et al., 2014).

65   Atmospheric processing of biomass burning OA during periods of low photochemical
66 activity (such as in winter or at night), known also as "dark" aging, has received substantially less
67 attention than photochemical processing. Recent aircraft measurements during agricultural
68 biomass burning periods indicated that nighttime oxidation of biomass burning VOCs is dominated
69 by NO_3 (Decker et al., 2019). Hartikainen et al. (2018) reported high amounts of nitrogen-
70 containing organic compounds both in the gas and particle phase after dark aging of residential
71 wood combustion emissions. Kodros et al. (2020) reported significant and rapid OOA production
72 in laboratory experiments in which fresh biomass burning emissions were exposed to NO_3 and
73 suggested that dark oxidation may be an important process on regional scales. In the same study,
74 ambient measurements in an urban area suggested that the mixing of O_3 from the residual layer
75 down to the nocturnal boundary layer can enhance the formation of NO_3 and the nighttime
76 oxidation of biomass burning emissions. The mixing of ozone from the residual layer and the
77 importance to nightime chemistry was also suggested in studies on nightime oxidation of biogenic
78 VOCs (Brown et al., 2009; Brown et al., 2013). Despite this important finding, the degree to which
79 biomass burning plumes undergo night-time aging and produce significant amounts of SOA
80 remains poorly understood. Lacking consideration of such nocturnal chemistry in transport models
81 has been suggested as a possible source of the under prediction oxidized organic aerosol mass by
82 a factor of 3-5 (Fountoukis et al., 2016; Tsimpidi et al., 2014) during wintertime in polluted areas
83 with low photochemical activity.

84   Usually smog chamber studies use fresh biomass burning emissions generated in the
85 laboratory by a single source as a starting point of their experiments. The use of a dual chamber
86 system with starting point ambient air rich in biomass burning emissions but also primary and
87 secondary pollutants from other sources offers a bridge between traditional laboratory studies and
88 ambient observations. Such a system offers the capability of aging realistic biomass burning
89 emissions from multiple sources and fuels, diluted in the atmosphere and mixed with other
90 pollutants (e.g., NO_x from transportation). In this study, we take advantage of the high levels of
91 OA from residential biomass burning in Patras, Greece (the country's third-largest city), to
92 investigate the importance of night-time chemistry in the processing of biomass burning OA.
93 Biomass burning leads to concentrations of OA exceeding 50 $\mu g\ m^{-3}$ in Patras in the early evening

94   (Florou et al., 2017). A dual atmospheric simulation chamber system is used to elucidate the

95   formation of SOA during winter periods in urban areas with high biomass burning organic aerosol

96   concentrations.

97

98   **2. Experimental Methods**

99   **2.1 Dual chamber system**

100   The dual chamber system developed by Kaltsonoudis et al. (2019) was used for

101   experiments in early 2020 in Patras, Greece during the PyroTRACH-PANACEA Wintertime 2020

102   experiment. The system consists of two 1.5 m^3 Teflon (PTFE) reactors attached to metallic frames.

103   Use of the second reactor as a reference (control chamber) allows the identification and potential

104   correction for any major experimental artifacts that could be due to the walls of the chamber and

105   the other complexities of this experimental system. The dual chamber system was deployed from

106   January 10 till February 15, 2020 in the city of Patras. The chambers along with the available

107   instrumentation were located indoors, in the campus of the University of Peloponnese,

108   approximately a few kilometers away from the center of the city (Figure S1). The windows of the

109   laboratory were kept open before and during the experiments, so the temperature of the dual

110   chamber system was in the 12-20°C range, while the outdoor temperature was on average 5 degrees

111   lower. The relative humidity (RH) in the chambers ranged from 35 to 45%.

112

113   **2.2 Experimental description**

114   Both chambers were flushed with ambient air before each experiment using a metal bellows

115   pump (Senior Aerospace, MB-602) for 1-2 h. This process is used to achieve higher sampling

116   efficiency and brings the system (chamber walls, tubing) close to equilibrium with ambient air

117   reducing losses of vapors to the sampling lines and walls of the chamber. Ambient air during

118   nighttime cold periods was introduced inside both chambers. In one of the chambers, (perturbed

119   chamber) ozone was added and upon reaction with the existing NO_x in the chamber formed NO_3

120   radicals. The second chamber (control chamber) was used as the reference in order to help us

121   understand the unperturbed evolution of the system inside the chamber. During all experiments

122   the chambers were under dark conditions. Ambient air was flushed through each of the chambers

123   with a flow of 80 L min^{-1}. More than 70% of the ambient PM was transferred to the chambers and

124   the concentrations of the measured VOCs were within 5% of their ambient values.

125   Using an automated valve switching between the two reactors, the particle and gas
126   concentrations in both chambers were measured. Data were collected 1.5 min after the switching
127   of the valve to avoid any memory effects related to the sampling lines. For the gas phase
128   measurements PTFE tubing (0.25 in) was used, while for the particle phase the tubing was copper
129   (0.25 in).

130   After filling the chambers with ambient air, the content of each chamber was characterized
131   for approximately one hour. The ozone added in the perturbed chamber after the characterization
132   period was in the range of 50-250 ppb. These values are higher than the 20 ppb measured during
133   the nighttime in Patras in this campaign, but some acceleration of the corresponding chemical
134   processes is necessary to reduce the effects of the walls and to limit the duration of the experiments
135   in the relatively small chambers used.

136   In selected experiments, approximately 40 ppb of d9-butanol was added in both chambers
137   to measure the OH concentration. Following Barnet et al. (2012), the OH concentration in the
138   chambers was estimated with the measured decay of the butanol concentration assuming a reaction
139   rate constant with OH of 3.4×10^{12} cm^3 $molecule^{-1}$ s^{-1}.

140   An incoherent broad-band cavity-enhanced absorption spectroscopy (IBB-CEAS) was
141   used to measure the NO_3 radical concentration. Detailed information about the technique can be
142   found elsewhere (Venables et al., 2006; Ventrillard-Courtillot et al., 2010; Chen and Venables,
143   2011; Fouqueau et al., 2020). Briefly the light from a LED source centered on the 662 nm
144   absorption cross section of NO_3 radical is focused and introduced into a high-finesse optical cavity
145   composed of two high reflectivity (~99.98%) and 1 m curvature mirrors. The optical cavity has a
146   length of 0.61 m and allows up to 4.5 km (at 662 nm) optical path and a detection limit up to 3 ppt
147   (integration time of 10 seconds). Particle-free air is passed through the cavity at 2.5 L min^{-1}.
148   Spectra between 640 and 685 nm were recorded with an OceanOptics QE-65 Pro spectrometer. A
149   time resolution of one minute was selected for these experiments. Calibration with NO_2 (800 ppb
150   in dry nitrogen, Air Liquide) was performed daily in order to precisely determine the reflectivity
151   of the mirrors and estimate the optical path. The sample spectra were fitted against standard spectra
152   of gas species absorbing in the spectral region of the instrument: NO_3 radical (Orphal et al., 2003),
153   NO_2 (Vandaele et al., 1998) and H_2O (reference spectrum recorded with the instrument) using the
154   DOASIS software.

A quadrupole proton-transfer reaction mass spectrometer (PTR-MS, Ionicon Analytik) was used to measure the concentration of VOCs including d9-butanol. We calculated the initial VOC levels in the chambers using the concentrations of m/z 42 (acetonitrile), 69 (isoprene), 71 (MVK & MACR), 73 (MEK), 79 (benzene), 93 (toluene) and 107 (xylene). We used the above m/z peaks, because the PTR-MS was calibrated for those values. For the experiments that the PTR-MS was not available we scaled the initial VOCs concentration using the black carbon (BC) levels. Using a series of gas monitors the concentration of nitrogen oxides (NO and NO_2) and ozone (O_3) were measured (Teledyne models: T201 and 400E respectively).

A TSI scanning mobility particle sizer (SMPS, classifier model 3080; DMA model 3081 CPC model 3775) was used for measuring the particle number distribution in the 15-700 nm range. An Aerodyne high-resolution time-of-flight aerosol mass spectrometer (HR-ToF-AMS) was measuring the composition and mass spectrum of OA. We did not use a dryer before the instruments and the RH of the samples was recorded. For the analysis of the HR-ToF-AMS data we used the AMS software toolkit (SQUIRREL v1.57I) and for the high-resolution data the Peak Integration by Key Analysis (PIKA v1.16I) software. The elemental ratios were calculated using the improved method of Canagaratna et al. (2015). The mass concentration and particle distribution of BC were measured using a single-particle soot photometer (SP2, Droplet Measurement Techniques).

The collection efficiency (CE) of the AMS was calculated applying the algorithm of Kostenidou et al. (2007), comparing the SMPS volume distributions and the AMS mass distributions. The CE ranged between 0.40-0.45 depending on the experiment. Using the same algorithm, the density of the OA was calculated to be in the range of 1.25-1.4 g cm^{-3}.

Using the theta (θ) angle (Kostenidou et al., 2009) a comparison between the OA spectra of the ambient and the chamber content after filling, we concluded that the OA composition injected in the chambers was the same as in the ambient air. The theta angle between the two chambers and the ambient OA spectra was always less than 4 degrees, suggesting excellent agreement. Also, the OA mass spectra in the two chambers right after their filling was in very good agreement (θ=3-4°), confirming that both chambers had the same OA composition initially. The θ angle is a useful metric for the comparison of OA mass spectra, similar to the often used R^2. A θ angle of two AMS spectra in the 0-5° range indicates an excellent match between the compared spectra, which should be considered identical for all practical purposes (R^2 ranging from 1 to 0.99).

For a θ angle of 6-10° there is a good match (R^2 approximately 0.98-0.96), but there are some small differences. A θ of 11-15° shows that the spectra are quite similar, but they are not the same (R^2: 0.95-0.92), while for a θ in the 16-30° range the spectra are coming from different sources, but there are some similarities (R^2: 0.91-0.73). A θ angle higher than 30° suggests clearly different AMS spectra. We use the θ angle in this study due to its ability to better represent relatively small differences than the coefficient of determination.

Following the completion of each perturbation experiment, a wall-loss characterization experiment was conducted to measure the size-dependent particle wall-loss rate constant inside the two chambers (Wang et al., 2018). The particles were produced by the atomization (TSI, model 3076) of an aqueous solution of ammonium sulfate (5 g L^{-1}). The ammonium sulfate seeds after the atomizer passed through a diffusion dryer and then were injected in the chambers without passing through a neutralizer. Using an ionizing fan, the chamber walls were swept before the start of each experiment to keep the particle loss rates low (Jorga et al., 2020).

The perturbation experiments started around 17:30-18:30 LT each evening (approximately 30 min after the sunset which during the campaign was from 17:00 to 18:00 LT), when the OA concentration was elevated from local nocturnal biomass burning emissions in the area for heating. The initial conditions in the experiments are summarized in Table 1. Thirteen experiments, eleven involving perturbation and two blank experiments, in which no ozone was injected in either chamber, were performed during January and February 2020 using ambient air from Patras.

3. Results

Our study was designed so that the experiments would start when biomass burning was the major source of both organic aerosol and VOCs. In this section we first present in detail the results of one typical experiment (Exp. 1) and then we summarize the results of the rest of the conducted experiments.

3.1 Results of a typical perturbation experiment

The average PM$_1$ concentration in the chambers during the filling process of Exp. 1 was approximately 50 μg m^{-3}. The concentration of OA during that period was 44 μg m^{-3} with 2.4 μg m^{-3} of BC. The positive matrix factorization (PMF) analysis of the full campaign ambient data set suggested that 70% of the OA at the time of filling originated from biomass burning. Other OA

217   sources included cooking OA or COA (15%), oxygenated OA or OOA (10%) and hydrocarbon-
218   like OA or HOA (5%). PMF was applied to the high resolution AMS organic mass spectra (m/z
219   up to 300) at 3 min resolution from the month long field campaign. Solutions with one to seven
220   factors were investigated. The best solution included 4 factors corresponding to BBOA, OOA,
221   COA and HOA. The time series of the four factors during the full field campaign are shown in
222   Figure S2. The detailed analysis of the field campaign, the determination of the PMF factors as
223   well as particle and gas measurements will be included in a forthcoming publication.

224   The initial concentration of O_3 in the two chambers was 10 ppb, of NO 17 ppb and of NO_2
225   24 ppb, values within 5% of their ambient concentrations. The measured initial VOC levels were
226   approximately 150 µg m^{-3} while the RH inside both chambers was approximately 45%. The rest
227   of the conditions are summarized in Table 1.

228   In Exp.1 NO_2 increased to 30 ppb in the perturbed chamber in approximately 30 min after
229   the ozone injection while at the same time NO levels dropped to close to zero. In the perturbed
230   chamber 2 hours after the injection the mixing ratio of NO_2 was 18 ppb and of ozone 220 ppb. In
231   the control chamber the concentrations of the above mentioned gases remained within 10% of their
232   initial levels. Due to the time needed for mixing and the rapid reaction of NO and O_3 it is difficult
233   to measure accurately the injected O_3 concentration. A zeroth order estimate can be made assuming
234   that the injected amount of ozone is equal to the final (equilibrated) amount of ozone in the
235   perturbed chamber plus the reacted NO_x (Table S1). Based on this zeroth order estimate, the
236   injected ozone in Exp. 1 was approximately 240 ppb.

237   Following the injection of ozone in the perturbed chamber (t=0 h) there was a rapid increase
238   of OA (Figure 1). Approximately 33 µg m^{-3} of SOA was produced in 2.5 hours (70% increase from
239   the initial injected OA levels). In just one hour after the injection of ozone, the OA concentration
240   increased by approximately 25 µg m^{-3}. This high rate secondary OA production rate of
241   approximately 25 µg m^{-3} h^{-1}is at least partially due to the high ozone levels used in these
242   experiments to accelerate the corresponding chemistry and reduce the problems caused by losses
243   of both particles and vapors to the walls of the chamber. Although this formation rate is true under
244   high ozone levels, the absolute increase in the OA concentration indicates the strong potential of
245   the ambient air in an urban area with strong biomass burning emissions to form SOA even under
246   dark conditions. The change of OA in the control chamber after the particle wall-loss corrections

247 was less than 7% at all times. This strongly indicates that the OA changes in the perturbation
248 chamber were not due to experimental artifacts.

249 The sulfate concentration remained practically the same (within 10%) in both the perturbed
250 and the control chambers after accounting for particle wall-losses. The initial nitrate in the
251 perturbed chamber was 1 µg m^{-3} more than in the control. This small difference can be an artifact
252 of the sampling system in this specific experiment. Production of approximately 6 µg m^{-3} of aerosol
253 nitrate was observed in the perturbed chamber with the majority of this increase in the form of
254 organic nitrate. Using the method described in Farmer et al. (2010) using the NO^+/NO_2^+ ratio from
255 the AMS, we estimate that close to 60% of the formed secondary aerosol nitrate in the perturbed
256 chamber was organic nitrate. Taking into account the organic nitrate, there was a 77% increase of
257 the OA compared to the initial concentration.

258 An increase of the ammonium concentration by close to 1 µg m^{-3} was observed in the
259 perturbed chamber (a 90% increase of ammonium compared to its levels before the injection of
260 ozone) while in the control chamber its concentration remained within 8% of the initial value.
261 Most of this increase was due to the formation of ammonium nitrate. Approximately 40% of the
262 total nitrate formed was inorganic nitrate, which requires approximately 1 µg m^{-3} of ammonium to
263 be neutralized. So the increase in ammonium is consistent with the increase in inorganic assuming
264 that ammonium nitrate was formed.

265

266 **3.2 Organic aerosol spectra**

267 Figure 2 represents the OA mass spectra in the two chambers at the start and end of Exp.1.
268 The comparison of the OA mass spectra in the perturbed chamber at the beginning (after the air
269 injection) and at the end (2.5 hours after the ozone injection) of Exp. 1 indicates that there was an
270 increase in the fractional signal of m/z: 28 (CO^+), 29 (CHO^+), 30 (CH_2O^+), 43 ($C_2H_3O^+$), and 44
271 (CO_2^+). The highest decrease was observed in 55 ($C_4H_7^+$), 57 ($C_4H_9^+$), 60 ($C_2H_4O_2^+$), 69 ($C_5H_9^+$),
272 91 ($C_7H_7^+$) and 95 ($C_7H_{11}^+$). The theta angle between the spectra was 19 degrees, indicating
273 significant change. The initial and final spectra in the control chamber had a θ angle of 8 degrees,
274 with changes in m/z 28, 44, 57 and 60.

275 The O:C ratio in the control chamber remained practically constant during Exp. 1, with a
276 value close to 0.4 (Figure 3). This suggests that there was relatively low chemical activity in this
277 chamber. This is consistent with the small change in the OA mass spectrum. This activity is could

278   be due to the existing O_3 and any produced NO_3 in the control chamber. On the contrary in the

279   perturbed chamber after the injection of ozone the O:C ratio increased rapidly reaching 0.52 after

280   30 min. At the end of the experiment, the O:C ratio in the perturbed chamber reached a value of

281   0.61, similar to the measured ambient value around 3:00 LT at night.

282   To calculate the mass spectrum of the produced OA in the perturbed chamber, we used a

283   simple mass balance approach. Details about this method can be found in Jorga et al. (2020).

284   Concisely, assuming that the main processes in the chamber are losses of particles to the chamber

285   walls and SOA formation, we estimate the initial (before the injection of ozone) and produced OA

286   mass spectra. Using the size-dependent particle loss rate constant measured at the end of each

287   experiment, the concentration of the pre-existing OA as a function of time can be calculated. The

288   pre-existing OA concentration in the perturbation chamber decreased from approximately 30 to 12

289    $\mu g\ m^{-3}$ during Exp. 1 (Figure 4). Additional information about the particle loss correction approach

290   together with the size dependence of the particle loss rate constants for Exp. 1 (Figure S3) can be

291   found in the SI. The produced SOA that remains suspended in the chamber is then the difference

292   between the total measured and the pre-existing or "initial" OA (Figure 4). The maximum

293   concentration of the produced SOA was 23 $\mu g\ m^{-3}$, but it was gradually reduced to 15 $\mu g\ m^{-3}$ due

294   to the particle losses to the walls. With the concentrations of the pre-existing OA and the produced

295   SOA both suspended in the chamber (these are the actual concentrations not corrected for wall

296   losses) the AMS spectra that correspond to the sum of the two, the spectrum of the produced SOA

297   can be estimated. Figure 5 shows the resulting spectra for the produced SOA both for Exp. 1 and

298   the average SOA spectra for all the experiments. The similarity of the spectra supports our choice

299   of Exp. 1 as representative of the rest.

300   Our estimation of the produced SOA levels is based on the mass balance approach of Jorga

301   et al. (2020) and not on the yields and concentration reduction of individual VOCs. Given the

302   uncertainties in the concentrations and the yields of the various VOCs and IVOCs in this complex

303   system this is a more accurate estimate. We assume that the main process responsible for the

304   reduction of the initial OA is loss of particles to the walls and that the loss of particle mass by

305   evaporation and then loss of the vapors to the walls is negligible. The accuracy of this assumption

306   can be confirmed by the change of the OA in the reference chamber (Figure 1a). The small change

307   of the particle wall loss-corrected OA concentration (less than 7%) supports our assumption. If

308   evaporation and vapor wall loss were important processes the corresponding concentration in the

309 reference chamber would be decreasing significantly. This is one of the advantages of our approach
310 using ambient air. The evaporation of the bbOA after its emission has already taken place in the
311 atmosphere. Therefore, the SOA production that we measure does account for the SVOCs that
312 have moved to the gas-phase as the bbOA gets diluted in the atmosphere. The changes in the
313 reference chamber illustrate well the changes that continue to happen in the system without our
314 acceleration of the chemistry.

315   The produced OA mass spectra from the perturbed chamber were compared with the
316 produced OA factor from the dark aging of biomass burning emissions in the laboratory (Kodros
317 et al., 2020). Although the present study deals with emissions from multiple biomass burning
318 sources and fuels in a complex air mixture and varying conditions compared to the laboratory work
319 (that used specific biomass burning emissions under idealized conditions) a comparison can
320 provide us with information about the consistency of the two studies. Kodros et al. (2020)
321 performed chamber experiments in which they exposed residential biomass burning emissions
322 from a residential wood stove to NO_2 and O_3 under different RH conditions. Here, we compare the
323 produced OA from a medium RH (approximately 45%) experiment with those of the ambient
324 perturbation experiments that had similar RH. The θ angle between the produced OA from
325 perturbation Exp.1 and the one from the laboratory chamber experiment was 11 degrees, indicating
326 a considerable degree of similarity (Figure 6). The comparison of our results with the work of
327 Kodros et al. (2020) can also be viewed as an independent test of the validity of our assumption
328 that most of the SOA formed in our experiments was indeed due to biomass burning. This previous
329 study used only biomass burning emissions therefore there is no doubt that their results represent
330 bbSOA. The good comparison of the produced SOA spectra in the two studies both strengthens
331 our argument that we mainly observe bbSOA formation and also strengthens the argument of
332 Kodros et al. (2020) that their laboratory results are a reasonable representation of realistic
333 atmospheric processing of biomass burning emissions.

334   The produced OA was also compared with the ambient oxygenated organic aerosol (OOA)
335 factor identified from the PMF analysis of the ambient data. The θ angle between the ambient
336 OOA in Patras from winter 2020 and the produced OA from Exp. 1 was 10 degrees. Similarities
337 were also observed in the produced OA and OOA from cities around the world during winter
338 periods. For Exp. 1 the θ angle was in the range of 9-18 degrees (Table S2) when compared with
339 OOA factors from Fresno, US (Ge et al., 2012), Barcelona, Spain (Mohr et al., 2012), Paris, France

340 (Crippa et al., 2013), Bologna, Italy (Gilardoni et al., 2016), Athens, Greece (Florou et al., 2017)

341 and Xi'an/Beijing, China (Elser et al., 2016). The contribution of biomass burning to the measured

342 OA in the above field studies ranged from 16% (Fresno, California) up to 70% (Patras and Athens,

343 Greece). The OOA as viewed by the PMF analysis of the AMS spectra has most of the time little

344 information about its source. Therefore, this similarity just strengthens our argument that the SOA

345 produced in our experiments was rather realistic. We further compared the AMS spectrum of the

346 SOA produced in this study with the spectra of the SOA produced during daytime oxidation of

347 biomass burning emissions. There are notable differences in the two spectra, with theta angles

348 approaching 30 degrees. This result is consistent with the findings of Kodros et al. (2020).

349

350 **3.3 Results of other experiments**

351 The rapid OA production observed during Exp. 1 was also observed in all the other

352 experiments, with approximately 75% of the produced OA formed in the first hour after the ozone

353 injection. The injected ozone levels in the other experiments, excluding Exp. 1 ranged from 65 to

354 220 ppb. Figure 7 shows the produced OA (including organic nitrates) in all the perturbation

355 experiments. In all experiments, the majority of secondary aerosol nitrate was organonitrate,

356 representing 55-85% of the total produced nitrate. Taking into account the organic nitrates, the

357 initial SOA formation rate in the perturbed chamber in the conducted experiments was on average

358 10 μg m^{-3} h^{-1}, ranging from 1 to 30 μg m^{-3} h^{-1}.

359 An increase in the O:C in the perturbed chamber was observed in all experiments with an

360 average increase from the initial O:C of 45% At the same time, the O:C in the control chamber

361 remained within 6% of the initial value. Table S3 summarizes the OA enhancement and the initial

362 and final O:C in the perturbed chamber in the conducted experiments.

363 The mass spectra of the produced OA in the perturbed chamber were similar to that of

364 Exp.1 with the major m/z values being 28, 29, 43, 44, 55 and 69 (Figure 5). The θ angle between

365 the different produced OA spectra in the perturbed experiments were less than 14 degrees,

366 suggesting similarities between the produced OA from the different perturbation experiments. The

367 θ angle between the produced OA mass spectra in the perturbed chamber and the one from Kodros

368 et al. (2020) was in the range of 9-16 degrees, suggesting similarity of the results of the two studies,

369 even if one relied on a single fuel burned in a single stove and the other in a mixture of emissions

370 from thousands of fireplaces and heating stoves. Another possible explanation of the difference

371 between the two studies is the presence of non-biomass burning emissions in the urban ambient
372 air that could contribute to the SOA formation.
373

374 **3.4 NO$_3$ and OH radical levels**

375   Based on the decay of d9-butanol after the injection of ozone, the OH concentration was
376 in the range of 0.2-0.4$\times10^6$ molecules cm^{-3} in the perturbation chamber suggesting that the addition
377 of ozone and reactions with organic vapors were not producing significant OH levels. Given the
378 sunlight in Greece even during the winter, these levels correspond to less than 10% of the daytime
379 OH in the area during that wintertime period. Despite the relatively low OH in the perturbation
380 chamber, its corresponding reactions with the various VOCs present do contribute to the observed
381 chemical changes. The characteristic reaction times with the OH of some of the VOCs present
382 (toluene, xylenes, isoprene, monoterpenes and phenol) that could contribute to SOA formation
383 ranged from approximately 9 to 160 hours suggesting that these reactions had a small contribution
384 to the rapid SOA formation observed during the first 30 min of a typical experiment (Figure 1).
385 The corresponding OH concentrations in the control chamber were practically zero and below the
386 detection levels of the d9-butanol approach. Measurements of the OH levels were only possible
387 when the PTR-MS was available (Exps 9-11), but the results were pretty consistent. Some OH
388 production is also expected in the ambient atmosphere as the ozone mixes in the nighttime
389 boundary layer from aloft, so these reactions are also taking place, albeit slowly, in the ambient
390 atmosphere too.

391   Nitrate radical concentrations above the detection level of a few ppt were only measured
392 in the perturbed chamber after the ozone injection. The maximum NO$_3$ radical concentrations in
393 the perturbed chamber ranged from 3 to 25 ppt with the highest observed during Exp. 8 (Table
394 S3). In this experiment before the ozone injection the NO$_3$ levels in both chambers were below the
395 detection limit of the instrument, while after the injection (t=0 h) the concentration of NO$_3$ started
396 to increase (Figure S4). In Exp. 8 there were 44 ppb of NO$_x$ initially and 150 ppb of O$_3$ were
397 injected. Approximately 15 μg m^{-3} of OA was formed in 2.5 h after the perturbation, with close to
398 2 μg m^{-3} of the OA formed being organic nitrate. The O:C reached a value of 0.6 at the end of this
399 experiment.

400   The measured NO_3 concentrations along with the low concentrations of OH in the

401   perturbed chamber suggests that the reactions of VOCs with NO_3 radicals and potentially ozone

402   were the major source of SOA production.

403

404   **3.5 Factors affecting the SOA production**

405   The highest produced SOA was observed, as expected, in experiments that had high initial

406   OA and VOC levels. Experiments 1, 4 and 6 had the highest measured inital VOC levels among

407   the conducted experiments, close to 150 μg m^{-3} (Table 1Figure). Although, only a fraction of the

408   VOCs present in the atmosphere were measured by the PTR-MS in this work, these measurements

409   provide an indication of the SOA formation potential of the corresponding air masses. We could

410   identify a strong link between the small variations in the speciation of the initial VOCs and the

411   SOA formed. This is probably due to the fact that we quantified only a small fraction of the VOCs

412   and IVOCs that serve as SOA precursors in the system.

413   The absolute concentration of SOA formed was also affected by the levels of NO present.

414   Experiments with low initial NO, less than 5 ppb, (Experiments 2, 3, 5 ,9 and 11) had the lowest

415   SOA production. The lowest NO_3 radical concentrations were also observed in those experiments.

416   This is due to the low NO_x availability in the atmosphere during these experiments. These low

417   NO_x levels result in low NO_3 levels in the perturbed chamber and therefore together with the

418   relatively low VOC levels, during the same periods, lead to low SOA production. Figure 8 shows

419   the correlation between the concentration of NO_3 radicals and the produced organic nitrate levels

420   in the perturbed chamber. The good correlation (R^2=0.79) supports the strong link between the

421   NO_3 chemistry occurring in the perturbed chamber and the corresponding SOA production. This

422   suggests that the oxidants levels (mainly NO_3) produced after reactions of ozone with the pre-

423   existing NO_x are affecting significantly the levels of SOA formed under these conditions. We

424   estimated an R^2=0.66 between the formed SOA and the levels of NO_3 in the perturbed chamber

425   (Figure S5).

426

427   **4. Conclusions**

428   In this work, we studied the nighttime aging of urban wintertime air, strongly influenced

429   by biomass burning emissions in Patras, Greece. Using a dual chamber system and ambient air as

430   a starting point, we injected additional ozone in only one chamber to accelerate nitrate radical

431 production via reactions with the pre-existing NO_x. The other chamber was used as a reference
432 mainly as a safeguard against potential experimental artifacts. The novelty of this experimental
433 approach is that it allowed the quantification of the nighttime chemical transformations of realistic
434 biomass burning emissions from thousands of sources and multiple fuels after they had been
435 diluted and mixed with ambient air. Our experiments took place during periods in which biomass
436 burning was responsible for 70% on average of the ambient OA and therefore the biomass burning
437 emissions were the dominant source of VOCs and IVOCs.

438   After the addition of ozone, rapid SOA formation was observed in the perturbed chamber
439 with the additional OA formed reaching up to 35 μg m^{-3}. The SOA formed increased the pre-
440 existing OA by 20-70%. Most of the secondary nitrate formed was organic nitrate, in some cases
441 reaching up to 85% of the total aerosol nitrate. On average 10% of the total OA formed was organic
442 nitrate. The organic aerosol formation was rapid, with 75% of the produced OA formed in the first
443 hour after the ozone injection. The organic aerosol content in the control chamber remained within
444 10% of the initial levels, suggesting limited chemical oxidation without the addition of ozone in
445 these timescales. These results strongly suggest that significant secondary OA can be formed even
446 during the nighttime of winter periods through the chemical processing of biomass burning
447 emissions.

448   The O:C of organic aerosol increased rapidly in the perturbed chamber following the ozone
449 injection. In 2-3 h of reactions a 40-50% increase of the O:C was observed while the OA O:C in
450 the control chamber remained within approximately 5% of the initial value. The produced OA
451 mass spectra showed similarities with the produced OA factor from dark aging biomass burning
452 experiments under laboratory conditions, pointing towards the important role of biomass burning
453 emissions in the OA formed in a winter urban environment. Furthermore, the produced SOA mass
454 spectra were quite similar to those of ambient oxygenated OA factors found in urban areas during
455 winter periods in which the fresh bbOA contributed 15-70% of the OA.

456   Nitrate radicals were observed only in the perturbed chamber and only after the ozone
457 injection. Their levels reached up to 25 ppt. The low and steady levels of hydroxyl radical in the
458 perturbed chamber along with the high characteristic reactions times of the measured VOCs with
459 the OH compared to the duration of the experiments, indicates that reaction with nitrate radicals
460 and ozone were responsible for the SOA formation and the change in the OA composition.

461

462 *Author Contribution*: S.D.J., K.F., C.K., J.K.K. and C.V. conducted the experiments, collected and
463 analyzed the data. S.N.P and A.N. conceived and directed the study. M.C., A.F. and B.P.-V.
464 provided the IBB-CEAS. S.D.J. and S.N.P. wrote the manuscript with inputs from all co-authors.
465
466 *Data availability*: Data related to this article are available upon request to the corresponding author.
467 The data will be available in the EUROCHAMP-2020 website.
468
469 *Competing interests*: The authors declare that they have no conflict of interest.
470

Acknowledgements

472 This work was supported by the European Union's Horizon 2020 EUROCHAMP–2020
473 Infrastructure Activity (grant agreement 730997) and project PyroTRACH (ERC-2016-COG)
474 funded from H2020-EU.1.1. - Excellent Science - European Research Council (ERC), project ID
475 726165. We thank Prof. A. Papalou and the University of Peloponnese for providing the space for
476 our experiments.

References

Ahern, A. T., Robinson, E. S., Tkacik, D. S., Saleh, R., Hatch, L. E., Barsanti, K. C., Stockwell, C. E., Yokelson, R. J., Presto, A. A., Robinson, A. L., Sullivan, R. C. and Donahue, N. M.: Production of secondary organic aerosol during aging of biomass burning smoke from fresh fuels and its relationship to VOC precursors, J. Geophys. Res., 124, 3583–3606, 2019.

Akagi, S. K., Yokelson, R. J., Wiedinmyer, C., Alvarado, M. J., Reid, J. S., Karl, T., Crounse, J. D. and Wennberg, P. O.: Emission factors for open and domestic biomass burning for use in atmospheric models, Atmos. Chem. Phys., 11, 4039–4072, 2011.

Akherati, A., He, Y., Coggon, M. M., Koss, A. R., Hodshire, A. L., Sekimoto, K., Warneke, C., De Gouw, J., Yee, L., Seinfeld, J. H., Onasch, T. B., Herndon, S. C., Knighton, W. B., Cappa, C. D., Kleeman, M. J., Lim, C. Y., Kroll, J. H., Pierce, J. R. and Jathar, S. H.: Oxygenated aromatic compounds are important precursors of secondary organic aerosol in biomass-burning emissions, Environ. Sci. Technol., 54, 8568–8579, 2020.

491   Alfarra, M. R., Prevot, A. S. H., Szidat, S., Sandradewi, J., Weimer, S., Lanz, V. A., Schreiber, D.,
492   Mohr, M. and Baltensperger, U.: Identification of the mass spectral signature of organic
493   aerosols from wood burning emissions, Environ. Sci. Technol., 41, 5770–5777, 2007.

494   Andreae, M. O. and Merlet, P.: Emission of trace gases and aerosols from biomass burning, Global
495   Biogeochem. Cycles, 15, 955–966, 2001.

496   Bond, T. C., Streets, D. G., Yarber, K. F., Nelson, S. M., Woo, J. H. and Klimont, Z.: A technology-
497   based global inventory of black and organic carbon emissions from combustion, J.
498   Geophys. Res., 109, D14203, doi:10.1029/2003JD003697, 2004.

499   Bougiatioti, A., Stavroulas, I., Kostenidou, E., Zarmpas, P., Theodosi, C., Kouvarakis, G.,
500   Canonaco, F., Prévôt, A. S. H., Nenes, A., Pandis, S. N. and Mihalopoulos, N.: Processing
501   of biomass-burning aerosol in the eastern Mediterranean during summertime, Atmos.
502   Chem. Phys., 14, 4793–4807, 2014.

503   Boy, J., Rollenbeck, R., Valarezo, C. and Wilcke, W.: Amazonian biomass burning-derived acid
504   and nutrient deposition in the north Andean montane forest of Ecuador, Global
505   Biogeochem. Cycles, 22, GB4011, 2008.

506   Brown, S. S., deGouw, J. A., Warneke, C., Ryerson, T. B., Dubé, W. P., Atlas, E., Weber, R. J.,
507   Peltier, R. E., Neuman, J. A., Roberts, J. M., Swanson, A., Flocke, F., McKeen, S. A.,
508   Brioude, J., Sommariva, R., Trainer, M., Fehsenfeld, F. C., and Ravishankara, A. R.:
509   Nocturnal isoprene oxidation over the Northeast United States in summer and its impact
510   on reactive nitrogen partitioning and secondary organic aerosol, Atmos. Chem. Phys., 9,
511   3027–3042, 2009

512   Brown, S. S., Dubé, W. P., Bahreini, R., Middlebrook, A. M., Brock, C. A., Warneke, C., de Gouw,
513   J. A., Washenfelder, R. A., Atlas, E., Peischl, J., Ryerson, T. B., Holloway, J. S., Schwarz,
514   J. P., Spackman, R., Trainer, M., Parrish, D. D., Fehshenfeld, F. C., and Ravishankara, A.
515   R.: Biogenic VOC oxidation and organic aerosol formation in an urban nocturnal boundary
516   layer: aircraft vertical profiles in Houston, TX, Atmos. Chem. Phys., 13, 11317–11337,
517   2013.

518   Bruns, E. A., El Haddad, I., Slowik, J. G., Kilic, D., Klein, F., Baltensperger, U. and Prévôt, A. S.
519   H.: Identification of significant precursor gases of secondary organic aerosols from
520   residential wood combustion, Sci. Rep., 6, 27881, 2016.

521 Canagaratna, M. R., Jimenez, J. L., Kroll, J. H., Chen, Q., Kessler, S. H., Massoli, P., Hildebrandt
522   Ruiz, L., Fortner, E., Williams, L. R., Wilson, K. R., Surratt, J. D., Donahue, N. M., Jayne,
523   J. T. and Worsnop, D. R.: Elemental ratio measurements of organic compounds using
524   aerosol mass spectrometry: characterization, improved calibration, and implications,
525   Atmos. Chem. Phys., 15, 253–272, 2015.

526 Capes, G., Johnson, B., McFiggans, G., Williams, P. I., Haywood, J. and Coe, H.: Aging of
527   biomass burning aerosols over West Africa: Aircraft measurements of chemical
528   composition, microphysical properties, and emission ratios, J. Geophys. Res., 113, 1–13,
529   2008.

530 Crippa, M., DeCarlo, P. F., Slowik, J. G., Mohr, C., Heringa, M. F., Chirico, R., Poulain, L.,
531   Freutel, F., Sciare, J., Cozic, J., Di Marco, C. F., Elsasser, M., Nicolas, J. B., Marchand,
532   N., Abidi, E., Wiedensohler, A., Drewnick, F., Schneider, J., Borrmann, S., Nemitz, E.,
533   Zimmermann, R., Jaffrezo, J.-L., Prévôt, A. S. H. and Baltensperger, U.: Wintertime
534   aerosol chemical composition and source apportionment of the organic fraction in the
535   metropolitan area of Paris, Atmos. Chem. Phys., 13, 961–981, 2013.

536 Decker, Z. C. J., Zarzana, K. J., Coggon, M., Min, K. E., Pollack, I., Ryerson, T. B., Peischl, J.,
537   Edwards, P., Dubé, W. P., Markovic, M. Z., Roberts, J. M., Veres, P. R., Graus, M.,
538   Warneke, C., De Gouw, J., Hatch, L. E., Barsanti, K. C. and Brown, S. S.: Nighttime
539   chemical transformation in biomass burning plumes: A box model analysis initialized with
540   aircraft observations, Environ. Sci. Technol., 53, 2529–2538, 2019.

541 Elser, M., Huang, R.-J., Wolf, R., Slowik, J. G., Wang, Q., Canonaco, F., Li, G., Bozzetti, C.,
542   Daellenbach, K. R., Huang, Y., Zhang, R., Li, Z., Cao, J., Baltensperger, U., El-Haddad, I.
543   and Prévôt, A. S. H.: New insights into $PM_{2.5}$ chemical composition and sources in two
544   major cities in China during extreme haze events using aerosol mass spectrometry, Atmos.
545   Chem. Phys., 16, 3207–3225, 2016.

546 Farmer, D. K., Matsunaga, A., Docherty, K. S., Surratt, J. D., Seinfeld, J. H., Ziemann, P. J. and
547   Jimenez, J. L.: Response of an aerosol mass spectrometer to organonitrates and
548   organosulfates and implications for atmospheric chemistry, Proc. Natl. Acad. Sci.., 107,
549   6670–6675, 2010.

550 Favez, O., El Haddad, I., Piot, C., Boréave, A., Abidi, E., Marchand, N., Jaffrezo, J.-L., Besombes,
551   J.-L., Personnaz, M.-B., Sciare, J., Wortham, H., George, C. and D'Anna, B.: Inter-

552  comparison of source apportionment models for the estimation of wood burning aerosols
553  during wintertime in an Alpine city (Grenoble, France), Atmos. Chem. Phys., 10, 5295–
554  5314, 2010.

555 Florou, K., Papanastasiou, D. K., Louvaris, E., Kaltsonoudis, C., Patoulias, D., Pikridas, M.,
556  Gkatzelis, G. I., Pandis, S. N. and Mihalopoulos, N.: The contribution of wood burning and
557  other pollution sources to wintertime organic aerosol levels in two Greek cities, Atmos.
558  Chem. Phys., 17, 3145–3163, 2017.

559 Ford, B., Val Martin, M., Zelasky, S. E., Fischer, E. V., Anenberg, S. C., Heald, C. L. and Pierce,
560  J. R.: Future fire impacts on smoke concentrations, visibility, and health in the contiguous
561  United States, GeoHealth, 2, 229–247, 2018.

562 Fouqueau, A., Cirtog, M., Cazaunau, M., Pangui, E., Zapf, P., Siour, G., Landsheere, X., Méjean,
563  G., Romanini, D., and Picquet-Varrault, B.: Implementation of an incoherent broadband
564  cavity-enhanced absorption spectroscopy technique in an atmospheric simulation chamber
565  for in situ NO3 monitoring: characterization and validation for kinetic studies, Atmos.
566  Meas. Tech., 13, 6311–6323, 2020.

567 Fountoukis, C., Megaritis, A. G., Skyllakou, K., Charalampidis, P. E., Denier van der Gon, H. A.
568  C., Crippa, M., Prévôt, A. S. H., Fachinger, F., Wiedensohler, A., Pilinis, C. and Pandis, S.
569  N.: Simulating the formation of carbonaceous aerosol in a European Megacity (Paris)
570  during the MEGAPOLI summer and winter campaigns, Atmos. Chem. Phys., 16, 3727–
571  3741, 2016.

572 Fuller, G. W., Tremper, A. H., Baker, T. D., Yttri, K. E. and Butterfield, D.: Contribution of wood
573  burning to PM10 in London, Atmos. Environ., 87, 87–94, 2014.

574 Ge, X., Setyan, A., Sun, Y. and Zhang, Q.: Primary and secondary organic aerosols in Fresno,
575  California during wintertime: Results from high resolution aerosol mass spectrometry, J.
576  Geophys. Res., 117, D19301, doi:10.1029/2012JD018026, 2012.

577 Gilardoni, S., Massoli, P., Paglione, M., Giulianelli, L., Carbone, C., Rinaldi, M., Decesari, S.,
578  Sandrini, S., Costabile, F., Gobbi, G. P., Pietrogrande, M. C., Visentin, M., Scotto, F.,
579  Fuzzi, S. and Facchini, M. C.: Direct observation of aqueous secondary organic aerosol
580  from biomass-burning emissions, Proc. Natl. Acad. Sci., 113, 10013–10018, 2016.

581 Hartikainen, A., Yli-Pirilä, P., Tiitta, P., Leskinen, A., Kortelainen, M., Orasche, J., Schnelle-
582  Kreis, J., Lehtinen, K. E. J., Zimmermann, R., Jokiniemi, J. and Sippula, O.: Volatile

583   organic compounds from logwood combustion: Emissions and transformation under dark

584   and photochemical aging conditions in a smog chamber, Environ. Sci. Technol., 52, 4979–

585   4988, 2018.

586 Hennigan, C. J., Miracolo, M. A., Engelhart, G. J., May, A. A., Presto, A. A., Lee, T., Sullivan, A.

587   P., McMeeking, G. R., Coe, H., Wold, C. E., Hao, W.-M., Gilman, J. B., Kuster, W. C., de

588   Gouw, J., Schichtel, B. A., Collett, J. L., Kreidenweis, S. M. and Robinson, A. L.: Chemical

589   and physical transformations of organic aerosol from the photo-oxidation of open biomass

590   burning emissions in an environmental chamber, Atmos. Chem. Phys., 11, 7669–7686,

591   2011.

592 Jolleys, M. D., Coe, H., McFiggans, G., Taylor, J. W., O'Shea, S. J., Le Breton, M., Bauguitte, S.

593   J.-B., Moller, S., Di Carlo, P., Aruffo, E., Palmer, P. I., Lee, J. D., Percival, C. J. and

594   Gallagher, M. W.: Properties and evolution of biomass burning organic aerosol from

595   Canadian boreal forest fires, Atmos. Chem. Phys., 15, 3077–3095, 2015.

596 Jorga, S. D., Kaltsonoudis, C., Liangou, A. and Pandis, S. N.: Measurement of formation rates of

597   secondary aerosol in the ambient urban atmosphere using a dual smog chamber system,

598   Environ. Sci. Technol., 54, 1336–1343, 2020.

599 Kaltsonoudis, C., Jorga, S. D., Louvaris, E., Florou, K. and Pandis, S. N.: A portable dual-smog-

600   chamber system for atmospheric aerosol field studies, Atmos. Meas. Tech., 12, 2733–2743,

601   2019.

602 Kodros, J. K., Papanastasiou, D. K., Paglione, M., Masiol, M., Squizzato, S., Florou, K.,

603   Skyllakou, K., Kaltsonoudis, C., Nenes, A. and Pandis, S. N.: Rapid dark aging of biomass

604   burning as an overlooked source of oxidized organic aerosol, Proc. Natl. Acad. Sci., 52,

605   33028-33033, 2020.

606 Kostenidou, E., Pathak, R. K. and Pandis, S. N.: An algorithm for the calculation of secondary

607   organic aerosol density combining AMS and SMPS data, Aerosol Sci. Technol., 41, 1002–

608   1010, 2007.

609 Kostenidou, E., Lee, B. H., Engelhart, G. J., Pierce, J. R. and Pandis, S. N.: Mass spectra

610   deconvolution of low, medium, and high volatility biogenic secondary organic aerosol,

611   Environ. Sci. Technol., 43, 4884–4889, 2009.

612 Mohr, C., DeCarlo, P. F., Heringa, M. F., Chirico, R., Slowik, J. G., Richter, R., Reche, C.,

613   Alastuey, A., Querol, X., Seco, R., Peñuelas, J., Jiḿenez, J. L., Crippa, M., Zimmermann,

614   R., Baltensperger, U. and Prévôt, A. S. H.: Identification and quantification of organic

615   aerosol from cooking and other sources in Barcelona using aerosol mass spectrometer data,

616   Atmos. Chem. Phys., 12, 1649–1665, 2012.

617   O'Dell, K., Ford, B., Fischer, E. V. and Pierce, J. R.: Contribution of Wildland-Fire Smoke to US

618   PM 2.5 and Its Influence on Recent Trends, Environ. Sci. Technol., 53, 1797–1804, 2019.

619   Orphal, J., Fellows, C. E., and Flaud, P.-M.: The visible absorption spectrum of NO_3 measured by

620   high-resolution Fourier transform spectroscopy, J. Geophys. Res., 108, 4077,

621   doi:10.1029/2002JD002489, 2003.

622   Ortega, A. M., Day, D. A., Cubison, M. J., Brune, W. H., Bon, D., De Gouw, J. A. and Jimenez,

623   J. L.: Secondary organic aerosol formation and primary organic aerosol oxidation from

624   biomass-burning smoke in a flow reactor during FLAME-3, Atmos. Chem. Phys., 13,

625   11551–11571, 2013.

626   Robinson, A. L., Subramanian, R., Donahue, N. M., Bernardo-Bricker, A. and Rogge, W. F.:

627   Source apportionment of molecular markers and organic aerosol. 2. Biomass smoke,

628   Environ. Sci. Technol., 40, 7811–7819, 2006.

629   Sundarambal, P., Balasubramanian, R., Tkalich, P. and He, J.: Impact of biomass burning on

630   Ocean water quality in Southeast Asia through atmospheric deposition: Field observations,

631   Atmos. Chem. Phys., 10, 11323–11336, 2010.

632   Tkacik, D. S., Robinson, E. S., Ahern, A., Saleh, R., Stockwell, C., Veres, P., Simpson, I. J.,

633   Meinardi, S., Blake, D. R., Yokelson, R. J., Presto, A. A., Sullivan, R. C., Donahue, N. M.

634   and Robinson, A. L.: A dual-chamber method for quantifying the effects of atmospheric

635   perturbations on secondary organic aerosol formation from biomass burning emissions, J.

636   Geophys. Res., 122, 6043–6058, 2017.

637   Tsimpidi, A. P., Karydis, V. A., Pozzer, A., Pandis, S. N. and Lelieveld, J.: ORACLE (v1.0):

638   module to simulate the organic aerosol composition and evolution in the atmosphere,

639   Geosci. Model Dev., 7, 3153–3172, 2014.

640   Vakkari, V., Beukes, J. P., Dal Maso, M., Aurela, M., Josipovic, M. and van Zyl, P. G.: Major

641   secondary aerosol formation in southern African open biomass burning plumes, Nat.

642   Geosci., 11, 580–583, 2018.

643   Vandaele, A. C., Hermans, C., Simon, P. C., Carleer, M., Colin, R., Fally, S., Mérienne, M. F.,

644   Jenouvrier, A., and Coquart, B.: Measurements of the NO_2 absorption cross-section from

645   42 000 cm^{-1} to 10 000 cm^{-1} (238–1000 nm) at 220K and 294 K., J. Quant. Spectrosc. Radiat.

646   Transf., 59, 171–184, 1998.

647   Wang, N., Jorga, S. D., Pierce, J. R., Donahue, N. M. and Pandis, S. N.: Particle wall-loss

648   correction methods in smog chamber experiments, Atmos. Meas. Tech., 11, 6577–6588,

649   2018.

650   Watson, J. G.: Visibility: Science and regulation, J. Air Waste Manag. Assoc., 52, 628–713, 2002.

651   Yu, J., Cocker, D. R., Griffin, R. J., Flagan, R. C. and Seinfeld, J. H.: Gas-phase ozone oxidation

652   of monoterpenes: Gaseous and particulate products, J. Atmos. Chem., 34, 207–258, 1999.

653   Zhao, D. F., Kaminski, M., Schlag, P., Fuchs, H., Acir, I.-H., Bohn, B., Häseler, R., Kiendler-

654   Scharr, A., Rohrer, F., Tillmann, R., Wang, M. J., Wegener, R., Wildt, J., Wahner, A. and

655   Mentel, T. F.: Secondary organic aerosol formation from hydroxyl radical oxidation and

656   ozonolysis of monoterpenes, Atmos. Chem. Phys., 15, 991–1012, 2015.

657

658

659

660

661

662

663

664

665

666

667 **Table 1:** Initial conditions for the dual chamber experiments.

Exp.	Start Time (LT)	RH (%)	Temperature (°C)	BC (μg m⁻³)	OA (μg m⁻³)	% bbOA	O:C	NO (ppb)	NO₂ (ppb)	Total VOCsᵇ (μg m⁻³)
1	17:45	45	17	2.4	44	70	0.4	17	24	150
2	17:45	35	13	0.8	18	65	0.36	4	22	50
3	17:50	33	15	0.6	19	37	0.25	3	20	38
4	17:55	40	14	2.5	48	68	0.33	90	20	160
5	17:45	35	15	1.1	18	69	0.4	3	25	71
6	17:50	40	17	2.6	50	72	0.36	32	25	160
7	18:00	45	20	1.0	16	78	0.36	15	20	63
8	17:55	42	22	1.2	22	77	0.45	22	22	75
9	18:15	40	19	0.7	16	75	0.44	3	14	46
10	18:15	45	21	1.6	25	50	0.33	32	21	100
11	18:30	45	24	0.6	6	48	0.41	1	5	38
12ᵃ	18:00	32	21	2.1	6	65	0.37	3	15	131
13ᵃ	18:20	30	19	3.0	33	67	0.35	31	23	188

668
669 [a] Blank experiment.
670 [b] Sum of the VOCs quantified by the PTR-MS.
671

672

673

674

675

676

677

678

679
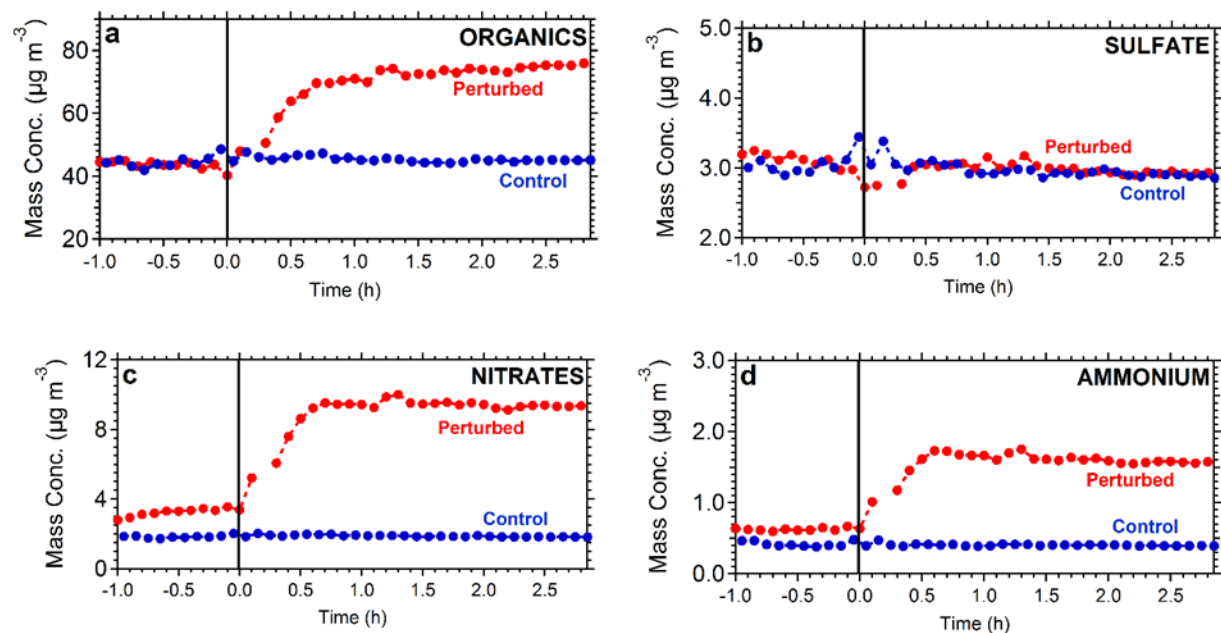
680 **Figure 1:** Particle wall-loss corrected aerosol mass concentration (CE=0.4) for the AMS-measured

681 (a) organics, (b) sulfate, (c) nitrates, and (d) ammonium in both the perturbed (red line) and the

682 control chamber (blue line) during Exp. 1.

683

684

685

686

687

688

689

690

691

692

693

694

695

696

697

698
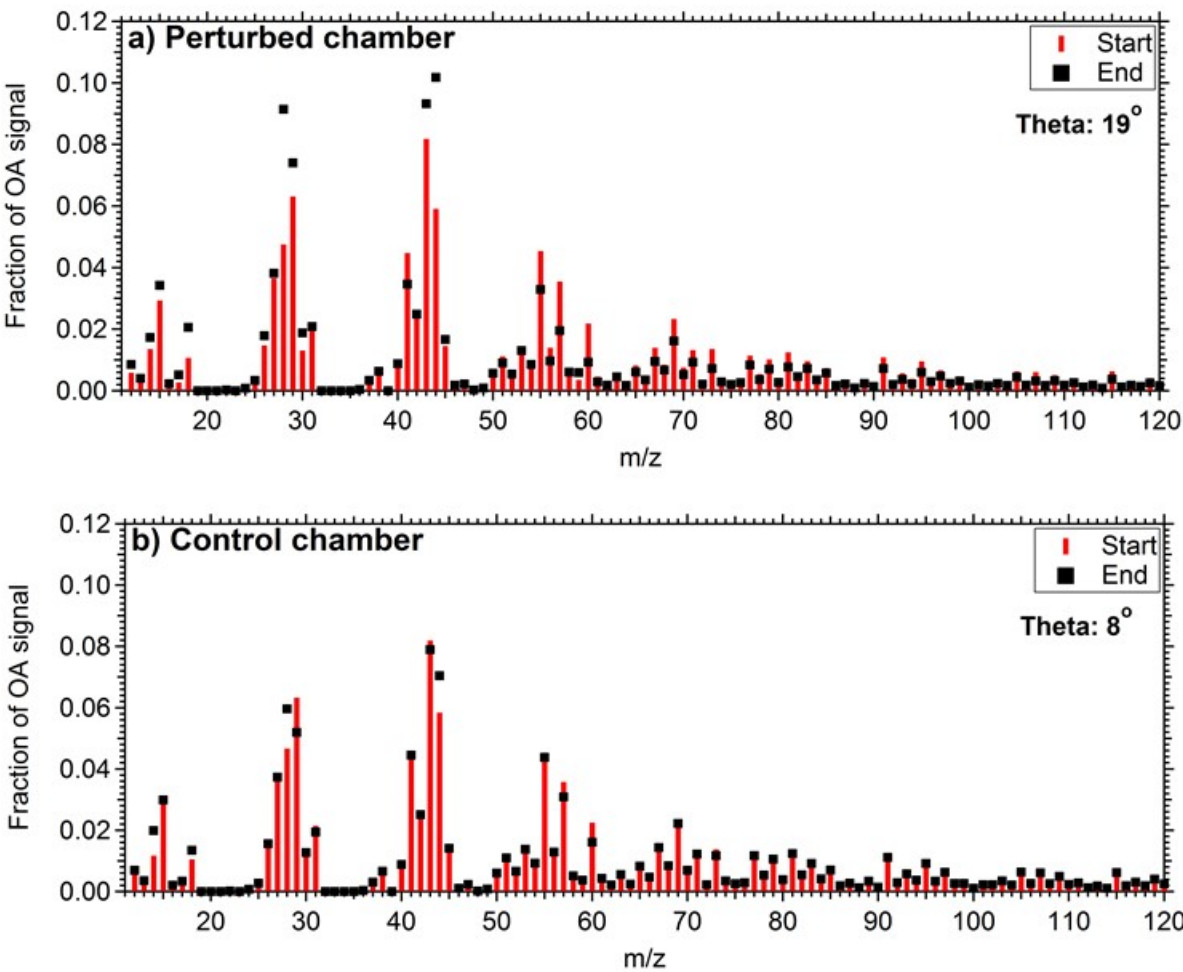
Figure 2: Mass spectra of OA during Exp. 1 in the (a) perturbed chamber and (b) control chamber

at the start of the experiment (after the filling process) and at the end of the experiment.

701

702

703

704
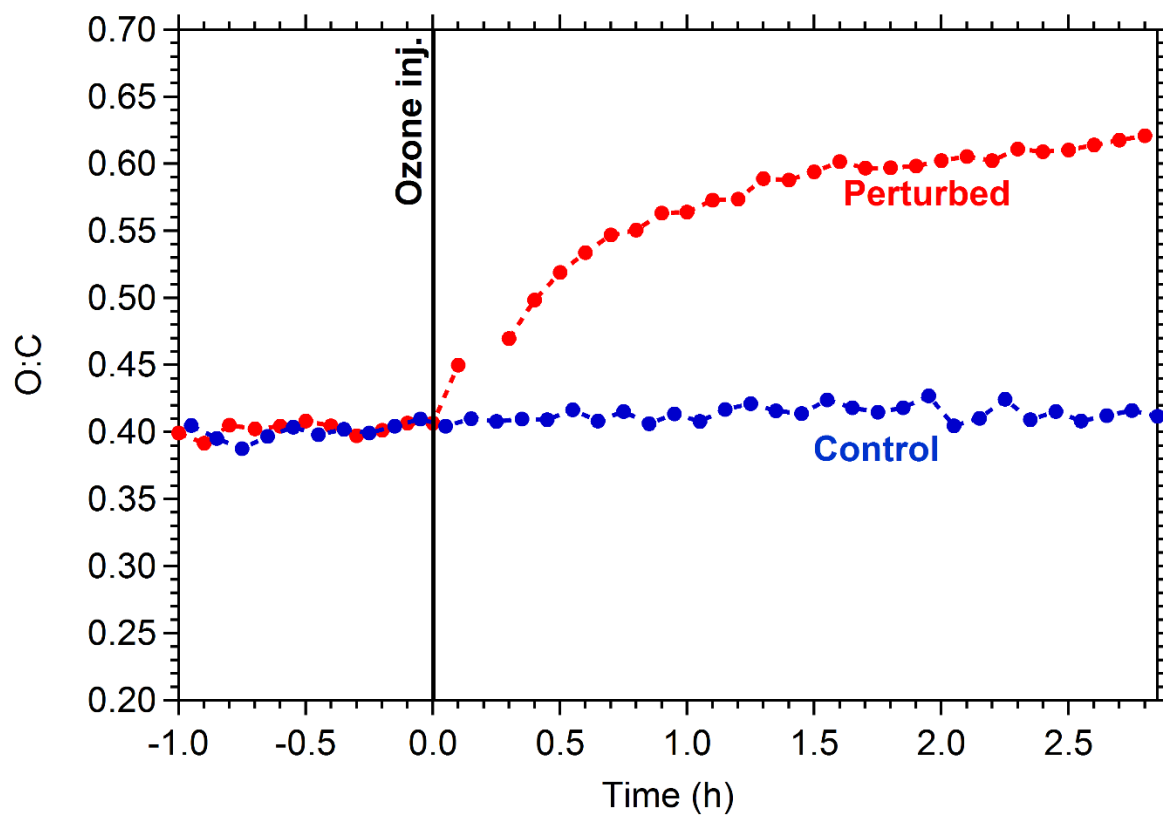
705 **Figure 3:** Oxygen to carbon ratio of the OA in the perturbed (red line) and the control chamber

706 (blue line) during Exp. 1.

707

708

709

710

711

712

713

714

715

716

717

718

719

720

721

722

723
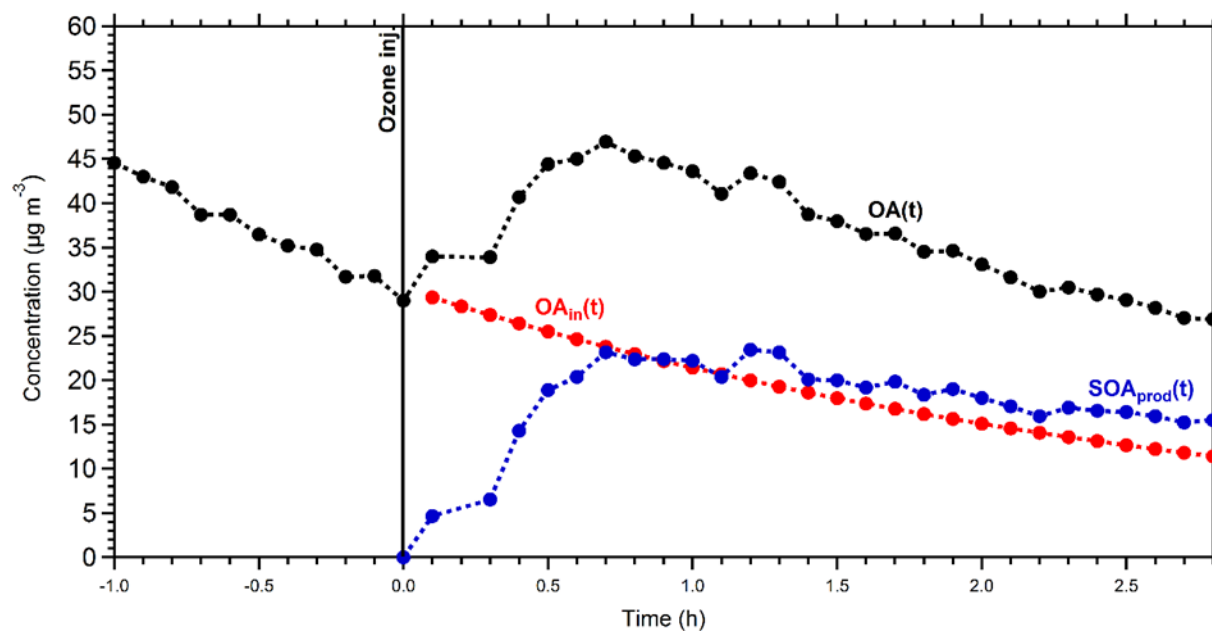
724 **Figure 4:** Mass concentration of the measured OA (black points), the initial OA (red points) and

725 the produced SOA (blue points) in the perturbed chamber in Exp. 1. All concentrations refer to the

726 suspended aerosol in the chamber and do not include the material deposited on the chamber walls.

727
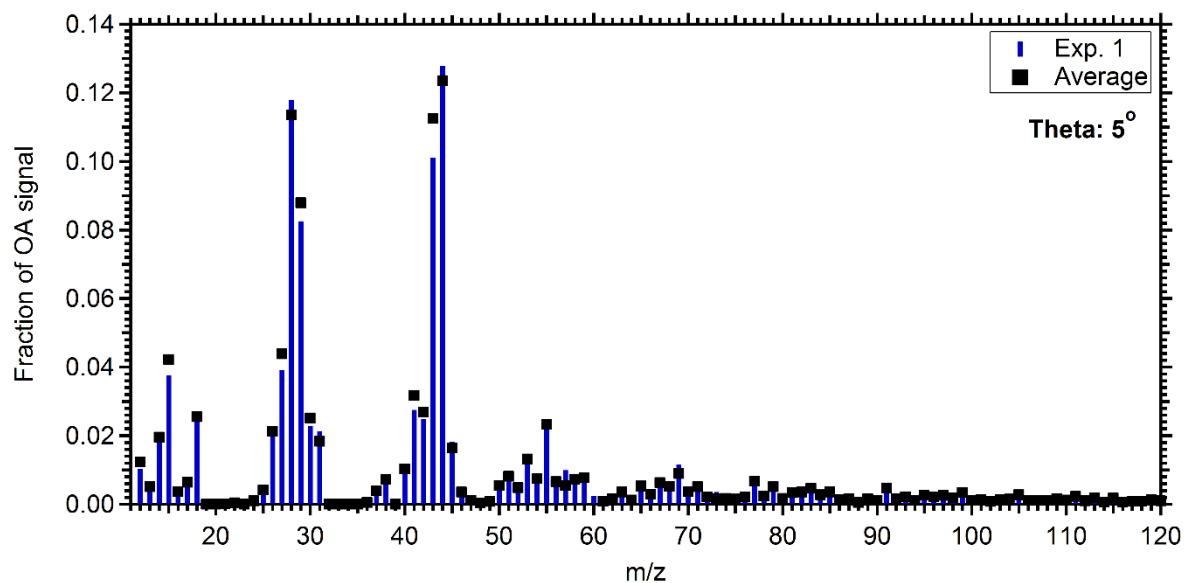
728 **Figure 5:** Mass spectrum of the produced SOA in the perturbed chamber for Exp. 1 (blue bars)

729 and the average spectrum of the produced SOA in all experiments (black squares).

730

731

732

733

734

735

736

737

738

739

740

741

742

743

744

745
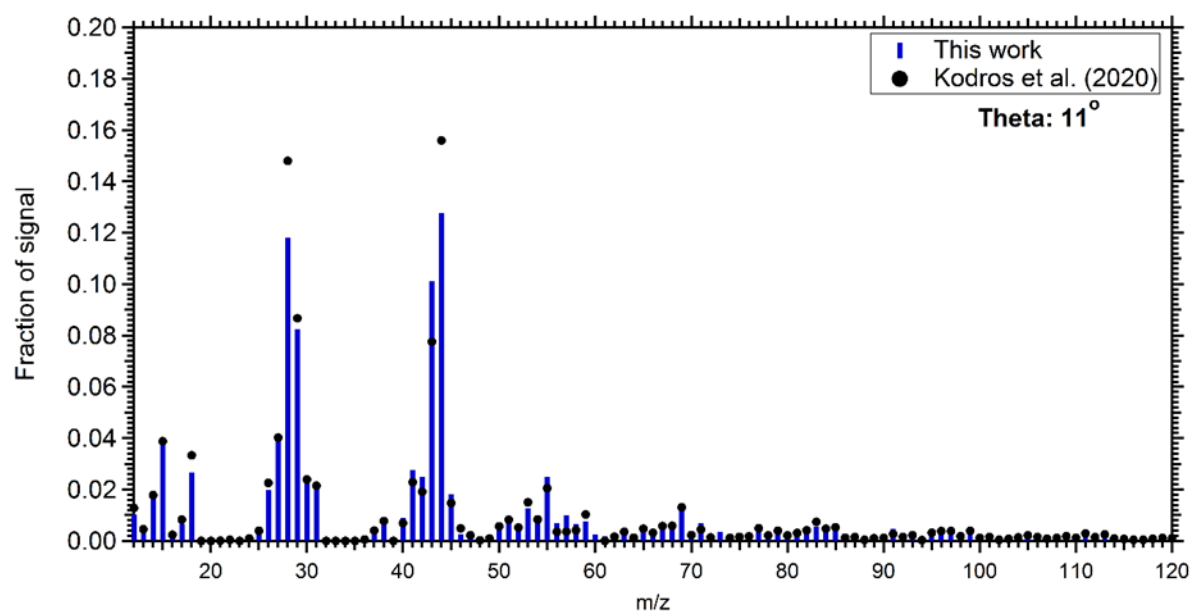
Figure 6: Comparison of the produced SOA mass spectra in the perturbed chamber during Exp. 1 (blue bars) and the produced SOA estimated during the chamber experiments of nocturnal aging of biomass burning emissions (Kodros et al. 2020) (black circles).

767

768
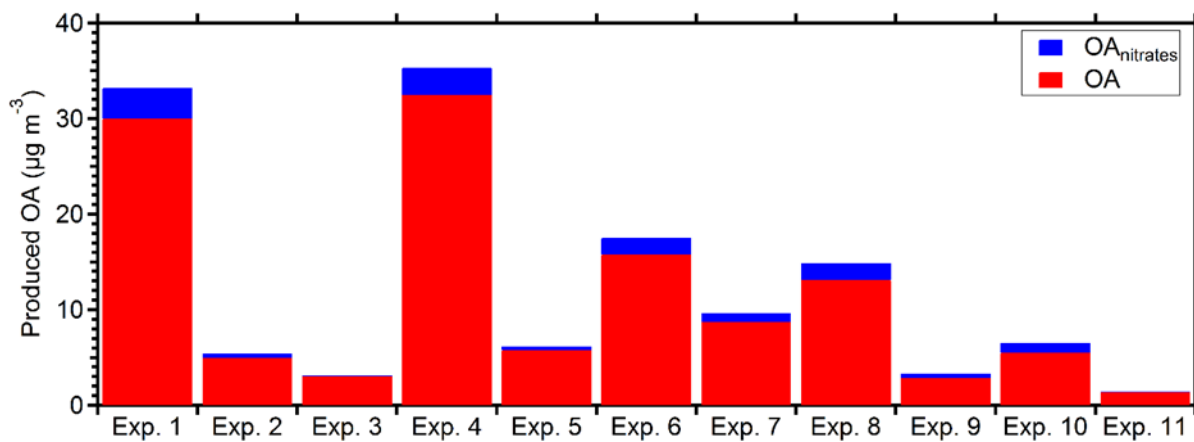
769 **Figure 7:** Produced OA (red bars) and the estimated organic nitrate (blue bars) in the perturbed
770 chamber for the eleven perturbation experiments. All values have been corrected for wall losses
771 and the AMS collection efficiency.

772

773

774

775

776

777

778

779

780

781

782

783

784

785

786

787

788

789
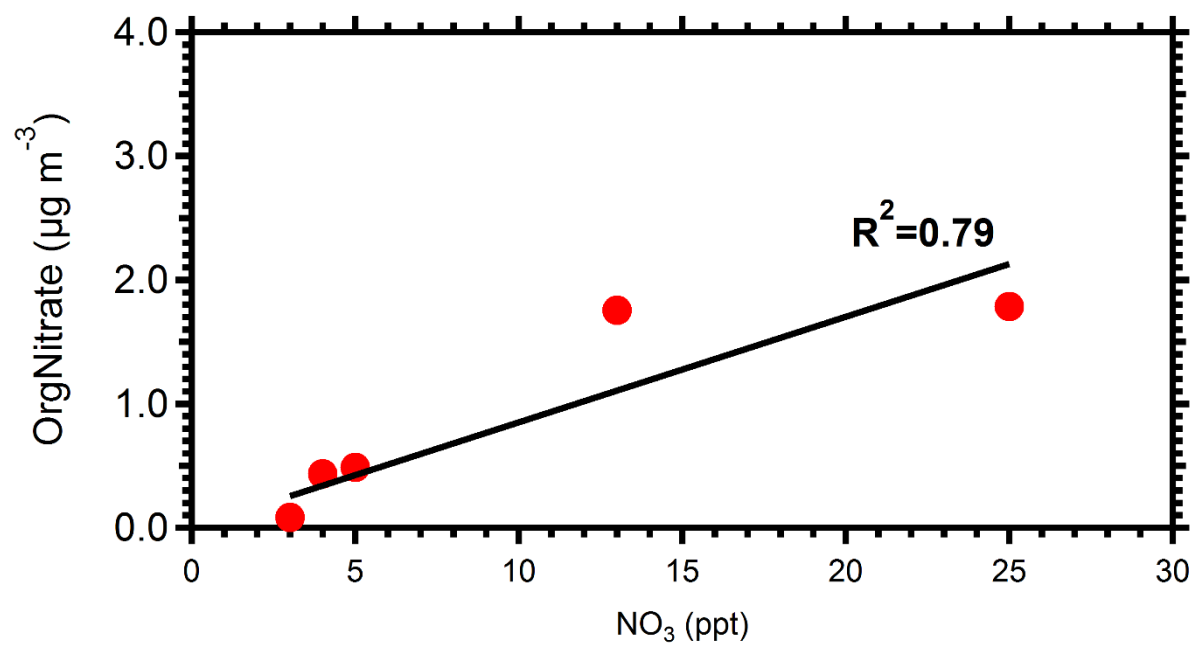
790   **Figure 8**: Correlation between NO_3 radicals with the organic nitrate formed in the perturbed

791   chamber.

792

793

794

795